A&A 591, A117 (2016)
DOI: 10.1051/0004-6361/201628665

Astronomy & Astrophysics

Deep *Herschel* PACS point spread functions[⋆,⋆⋆] *(Research Note)*

M. Bocchio[1], S. Bianchi[2], and A. Abergel[1]

[1] Institut d'Astrophysique Spatiale (IAS), UMR 8617, CNRS, Université Paris Saclay, Université Paris Sud, 91405 Orsay, France
e-mail: mbocchio@arcetri.astro.it
[2] INAF–Osservatorio Astrofisico di Arcetri, Largo Enrico Fermi 5, 50125 Firenze, Italy

Received 8 April 2016 / Accepted 11 May 2016

ABSTRACT

The knowledge of the point spread function (PSF) of imaging instruments represents a fundamental requirement for astronomical observations. The *Herschel* PACS PSFs delivered by the instrument control centre are obtained from observations of the Vesta asteroid, which provides a characterisation of the central part and, therefore, excludes fainter features. In many cases, however, information on both the core and wings of the PSFs is needed. With this aim, we combine Vesta and Mars dedicated observations and obtain PACS PSFs with an unprecedented dynamic range (~10^6) at slow and fast scan speeds for the three photometric bands.

Key words. instrumentation: photometers – techniques: image processing – techniques: photometric

1. Introduction

The response of a given imaging instrument to a point source is known as the point spread function (PSF). In the case of diffraction-limited space telescopes this quantity is dominated by the configuration of the aperture and it is key to many aspects of astrophysical observations. First, models are often compared to observations. This operation is typically carried out by convolving a given model to the PSF of the observed image. An error in the estimate of the PSF would lead to errors in the interpretation of the observations. Second, images taken with different instruments or at different wavelength bands intrinsically have distinct resolutions. In order to compare multiple images on a pixel-by-pixel basis they need to be smoothed to a common (larger) PSF, which is a procedure that involves the use of convolution kernels. The construction of a convolution kernel is based on the knowledge of the PSF of the image that needs to be processed and the common PSF. Third, the interface between different regions (e.g. photodissociation regions or the outskirts of galaxies) are often rich in information. A strong gradient in intensity usually characterises the interface, however, making the contrast between these regions very strong. Faint wings of the PSF of the instrument can extend very far from the PSF centre and if the contrast between regions is sufficiently high, faint structures of the PSF can have an intensity that is comparable to that of the fainter regions. This represents a possible source of contamination and needs to be carefully taken into account.

The PSF of the photometer of the PACS instrument (Poglitsch et al. 2010) on board *Herschel* is characterised by (Lutz 2015) a narrow core, a tri-lobe pattern, and knotty structured diffraction "rings" at sub-percent level. For fast scans in standard and parallel mode, this PSF structure due to the telescope is smeared by detector time constants and data averaging, resulting in a larger PSF. The PSFs delivered by the PACS instrument control centre (ICC) have been observed using the Vesta asteroid and provide information about the central part of the PSFs (until a radius of ~60″) at different scan speeds. Mars observations were used for the characterisation of the encircled energy fraction (EEF) in the wings of PSFs but were not combined with Vesta observations in the PSFs delivered. The goal of this Research Note is to combine Vesta and Mars dedicated observations to provide new estimates of the PACS PSFs with an unprecedented dynamic range (~10^6) to permit the proper characterisation of the central part and the wings.

This Research Note is organised as follows: in Sect. 2 we present the PACS observations, give details on the data processing followed, and describe the method used to produce the final PSFs. In Sect. 3 we analyse the PSFs and compare them to extragalactic images and, finally, in Sect. 4 we draw our conclusions.

2. Vesta and Mars PACS data processing

Herschel PACS dedicated PSF observations are scan maps centred on various objects taken at 70 (blue band), 100 (green band), and 160 (red band) μm. The core of the PSF is best characterised observing faint objects (e.g. the asteroid Vesta), while the wings of the PSF can only be seen in observations of bright objects (e.g. Mars). Using a combination of images of bright and faint objects, it is therefore possible to obtain a good characterisation of the PACS PSFs.

2.1. Observations and data reduction

We consider dual-band observations of Vesta and Mars (see obsIDs in Table 1) taken at the three different PACS wavelength bands and with a scan speed of 20″/s and 60″/s. The *Herschel*

⋆ *Herschel* is an ESA space observatory with science instruments provided by European-led Principal Investigator consortia and with important participation from NASA.
⋆⋆ FITS files of our PACS PSFs (Fig. 2) are only available at the CDS via anonymous ftp to cdsarc.u-strasbg.fr (130.79.128.5) or via http://cdsarc.u-strasbg.fr/viz-bin/qcat?J/A+A/591/A117

Table 1. ObsIDs of the available observations of Vesta and Mars.

Band	Scan speed	Vesta	Mars
Blue/red	20	1342195472	–
		1342195473	–
Blue/red	60	–	1342231157
		1342195470	1342231158
		1342195471	1342231159
		–	1342231160
Green/red	20	1342195476	–
		1342195477	–
Green/red	60	–	1342231161
		1342195474	1342231162
		1342195475	1342231163
		–	1342231164

interactive processing environment (HIPE; v.12.1.0; Ott 2010) was first used to bring the raw Level-0 data to Level-1 using the PACS calibration tree PACS_CAL_65_0 and the pipeline scripts for Solar System Objects (SSO). Maps were then produced using Scanamorphos (v.24.0, Roussel 2013) with pixel sizes of 1″ and rotated of the roll angle $\theta_{RA} = 292.44°$ and 108.6° clockwise (for Vesta and Mars observations, respectively) so as to have the Z-axis of the spacecraft point up.

Unfortunately, there are no sufficient dedicated observations in parallel mode that are useful for a correct characterisation of the PSF. We bypassed this problem partly simulating parallel-mode observations at 20″/s and 60″/s from observations in standard mode. This is performed by modifying the HIPE pipeline to average fluxes and coordinates of two consecutive frames of our data, therefore mimicking the reduced sampling frequency of the detectors (for the blue and green bands only) in parallel mode (Lutz, priv. comm.).

The observations considered have an array-to-map angle (ama) of ±42.4°, i.e. scan directions form an angle of ±42.4° with respect to the Z-axis of the spacecraft. This angle corresponds to the SPIRE "magic" angle[1] (Valtchanov 2014) and it is always used for observations in parallel mode. Observations in standard mode can be performed using an ama =±42.4° or ±63°.

The scanning direction does not affect the shape of the PSF for low scanning speeds (10 and 20″/s). On the contrary, Vesta images obtained at fast scanning speed (60″/s) present a clear elongation along the scanning direction. The central region of Mars images is saturated and no elongation is observed; Mars observations at lower scan speeds are therefore not required and images taken at 60″/s are used for the characterisation of the faint wings at both slow and fast scan speeds. In the *Herschel* Science Archive there is no PACS observation (apart from dedicated observations for PSFs analysis) at 60″/s in standard mode with an ama =±63°, we therefore consider only PSFs with ama =±42.4°. For the observations of Mars, the pixels centered on the source are heavily saturated, leading to significant trails. When using Scanamorphos (Lutz 2015) these artifacts are greatly reduced, masking the affected regions.

2.2. Merging observations

In order to produce PSFs for images obtained at low scan speeds (10 and 20″/s), we merge Vesta and Mars observations at 20″/s and 60″/s, respectively, while we use Vesta and Mars observations at 60″/s for PSFs for high scan speeds (60″/s). The same is done for the parallel mode, using the corresponding partly simulated data.

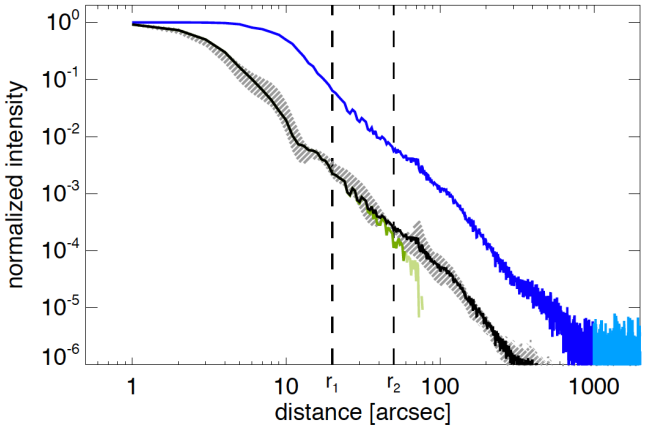

Fig. 1. Average radial profile of Vesta (green) and Mars (blue) observations and of the estimated PSF (black) for 70 μm images at a scan speed of 20″/s. The light green and light blue lines are Vesta and Mars profiles for $r > c_2$. The shaded region indicates the range of profiles along different directions of the estimated PSF. Vertical dashed black lines indicate r_1 and r_2.

First of all, we notice that Mars images have a good signal-to-noise ratios (S/N) up to ∼1000″ from the centre, while Vesta images are noisy for radii that are larger than 60″. We measure the background in Mars images and we remove it, while the background estimation for Vesta is computed with a more sophisticated technique (see Sect. 3.1). Images are then normalised so that the total integrated flux equals unity and the radial profile (averaged over the 2π angle) for both Vesta and Mars is computed (see Fig. 1 for an example at 70 μm with a scan speed of 20″/s). The central region of the Mars image is saturated and the ratio between the two profiles is constant over a given radial region (i.e. between $r_1 = 20''$ and $r_2 = 50''$ for observations in Fig. 1). To avoid introducing any artifacts in the PSFs, we then rescale the Mars images to those of Vesta and compute the PSF as

$$\mathrm{PSF}(r,\theta) = \begin{cases} V(r,\theta) & \text{if } r \le r_1 \\ V(r,\theta)[1-f(r)] + M(r,\theta)f(r) & \text{if } r_1 < r < r_2 \\ M(r,\theta) & \text{if } r \ge r_2, \end{cases} \quad (1)$$

where $V(r,\theta)$ and $M(r,\theta)$ indicate the Vesta and the rescaled Mars images, respectively, and

$$f(r) = 6\left(\frac{r-r_1}{r_2-r_1}\right)^5 - 15\left(\frac{r-r_1}{r_2-r_1}\right)^4 + 10\left(\frac{r-r_1}{r_2-r_1}\right)^3, \quad (2)$$

is a smooth Heaviside step function with null first and second derivatives at the extremes r_1 and r_2.

The average radial profile of the estimated PSF tightly follows that of Vesta at short radii, while it tends to the profile of Mars further from the centre (see Fig. 1). During the operation of merging, the information on the asymmetry of the PSF is not lost and radial profiles measured along different directions show rather strong variability with respect to the average radial profile (shaded region in Fig. 1).

We also tested for the impact of the finite size of Mars on the PSF determination. At the time of observations, the apparent diameter of the planet as seen from the L2 point[2] was $d_M \sim 5\farcs55$,

[1] Adopting an ama of ±42.4° provides a good coverage for fully sampled maps in the three SPIRE bands.

[2] Ephemerides can be accessed at: http://ssd.jpl.nasa.gov/?horizons

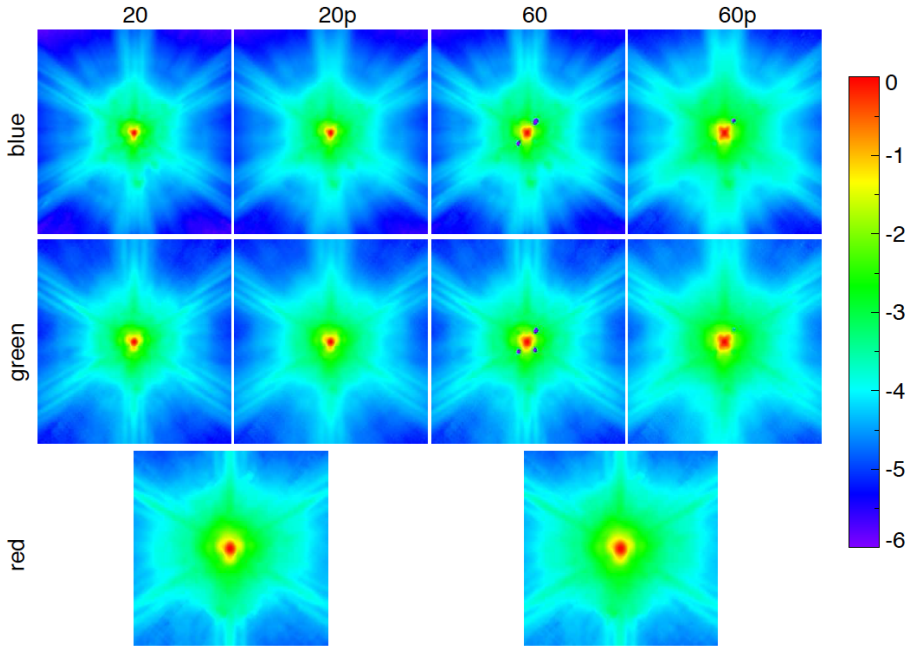

Fig. 2. Our estimates of PACS PSFs (in log scale) as a function of the filter and scan speed. All images are 300″ × 300″. Red band PSFs in standard and parallel modes are exactly the same. The spacecraft *Y*- and *Z*-axis are to the left and to the top, respectively.

which is comparable to the full width at half maximum (FWHM) of the PACS PSFs and therefore cannot be considered point-like. However, the core of PSFs is obtained from Vesta measurements and Mars observations are only used for the characterisation of the faint structures at $r > r_1$. When a circle of diameter $d_M \sim 5\farcs55$ is convolved with our composite PSFs, the profile of the resulting images for $r > r_1$ remains unchanged with respect to the PSFs. This demonstrates that the finite size of Mars does not affect the shape of the derived PSFs.

3. PSF analysis

3.1. Encircled energy

The EEF is computed using the same notation and following the method by the ICC (Lutz 2015) as follows:

$$EEF_{\rm obs}(r) = \frac{\int_0^r \int_0^{2\pi} [\mathrm{PSF}(r,\theta) - c_1]\, r \mathrm{d}r\, \mathrm{d}\theta - c_3}{\int_0^{c_2} \int_0^{2\pi} [\mathrm{PSF}(r,\theta) - c_1]\, r \mathrm{d}r\, \mathrm{d}\theta - c_3}, \quad (3)$$

where c_1 represents the background value to be removed from the observed image, c_2 is the maximum radius out to which we compute the EEF, and c_3 is the flux missing in the PSF core due to saturation.

We compute the EEF for the Vesta and Mars images (see Fig. 3) assuming $c_1 = 0$, $c_2 = 60''$ and $1000''$ for Vesta and Mars, respectively. We deduced the value of c_3 for Mars images by comparing the integrated observed flux to the nominal flux given by the ICC (i.e. $S[70] = 44\,670$ Jy, $S[100] = 24\,740$ Jy and $S[160] = 11\,160$ Jy). The observed fluxes are ∼37.5%, 53.6%, and 86.8% of the nominal values at 70, 100, and 160 μm, respectively.

However, the flux of Vesta for radii larger than c_2 is non-negligible and must be taken into account for the calculation of the EEF. Furthermore, since the S/N in Vesta maps is very low at $r > c_2$, the value of c_1 cannot be estimated directly from observations. From a visual comparison of the slope of the Vesta and Mars EEF, we find $c_1 \simeq 10^{-4}$ (normalised to the peak of the Vesta image) for all pairs of observations. The flux outside radius c_2 in Vesta observations is 8.3%, 9.8%, and 12.3% for blue, green, and red bands. We then correct the Vesta EEF for the flux lost due to the non-zero c_1 and the flux outside radius c_2 (dotted line in Fig. 3). The corrected EEF curve tightly follows that of Vesta at short radii and tends to that of Mars for $r \gtrsim 20''$. We finally compute the EEF for our estimate of the PACS PSF (solid line in Fig. 3) and note that it agrees very well with the corrected Vesta EEF, therefore supporting the methodology used. The EEF curve that we obtain is comparable to that presented by the PACS ICC (red dashed line in Fig. 3, Lutz 2015), with a little difference for $r \lesssim 2''$ due to the adopted centering technique.

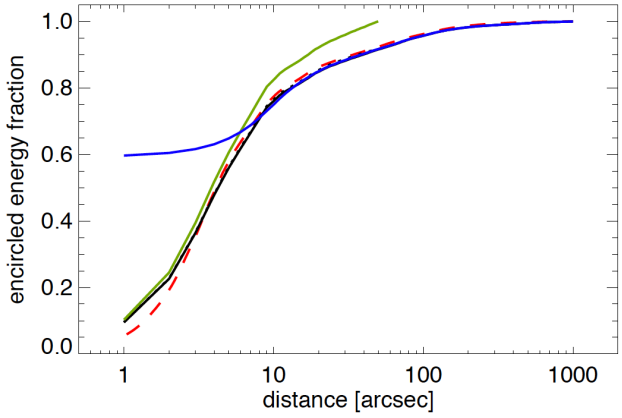

Fig. 3. Encircled energy fraction (blue band) for Vesta (green line), Mars (blue line), for the estimated PSF (solid black line), and as obtained by the ICC (red dashed line). The dotted black line indicates the corrected Vesta EEF (see text for details).

3.2. PSF profile

The computed PACS PSFs are presented in Fig. 2. They are not axisymmetric and are characterised by a large width variability depending on the direction. Using a two-dimensional (2D) Gaussian fit of the PSFs, we measure the FWHM along the *Y* and *Z* directions. The resulting values are reported in Table 2 and are comparable to those obtained by the PACS ICC (Lutz 2015). As

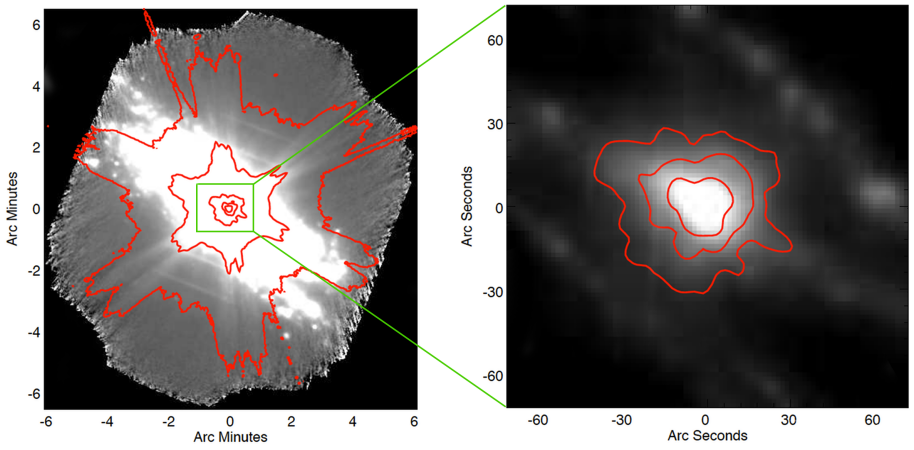

Fig. 4. PACS 70 μm observations of NGC 253 with overplotted contours of our PSF, rotated of an angle $\theta_{RA} \sim 114°$ clockwise (see text). *Right panel*, zoom to the central region.

Table 2. FWHM of the estimated PSFs in arcsec along the Y and Z directions.

Band	Dir.	Scan speed			
		20	20p	60	60p
Blue	Y	5.77	6.28	7.75	9.71
	Z	6.35	6.94	8.72	10.77
Green	Y	6.90	7.31	8.68	10.67
	Z	7.26	7.75	9.51	11.72
Red	Y	10.59		11.80	
	Z	12.29		13.70	

Notes. Scan speeds are indicated in arcsec/s, 20p and 60p are in parallel mode.

expected, the FWHM increases in both Y and Z directions from blue to red filters. PSF features are observed along the Z direction (see Fig. 2) and the width is therefore systematically larger (up to 20%) along this axis with respect to the Y direction. The scan speed contributes to the enlargement of the PSF and a clear elongation is visible towards the scanning direction (±42.4° with respect to the Z axis).

3.3. An example

Astronomical objects presenting a strong contrast between different regions can present evident PSF features. NGC 253 is a intermediate spiral galaxy currently undergoing an intense star formation. This galaxy has been observed by PACS at 70 and 160 μm at a scan speed of 20″/s and with the $+Z$ direction of the telescope rotated by an angle $\theta_{RA} \sim 114°$ west of north (clockwise). At these wavelengths, the central region of the galaxy is very bright compared to the rest of the galaxy, which is then contaminated by the lobes and faint structures of the PSFs.

Figure 4 illustrates the PACS 70 μm image of this galaxy with the contours of our estimated PSF overplotted. On the right panel, we show a zoom to the central region and overplot contours of the PSF core. Both the faint structures and core of the PSF dominate over the extended emission of the galaxy and match very well with the PSF[3]. This observation represents an example of a case where a good characterisation of the PSF of the instrument is needed to correctly interpret astrophysical data.

[3] The faint stripes visible in the left panel are due to crosstalk (Okumura 2010) and are not directly related to the shape of the PSF.

Similarly, our computed PACS PSFs were used in a recent study of the scale height of the dust distribution in a nearby edge-on galaxy, NGC 891 (Bocchio et al. 2016). The larger width of the PSFs compared to that of modelled PSFs for the "as built" telescope (Geis & Lutz 2009) and their radial asymmetry lead to a narrower dust scale height by up to a factor of ~60%.

4. Conclusions

Using dedicated observations of Vesta and Mars, we provide new estimates of the PACS PSFs for scan speeds of 20″/s and 60″/s both in standard and parallel mode. The obtained PSFs have a wide dynamic range (~10^6) enabling a proper characterisation of both the core and faint structures of the PSFs.

As an example we consider NGC 253, a galaxy with a strong contrast between the central and peripheral regions. From a comparison between our estimated PSFs and PACS observations of NGC 253, we obtain an excellent matching, therefore supporting the reliability of the method used.

Acknowledgements. We would like to acknowledge Prof. D. Lutz for a useful discussion and for giving us part of the code needed to simulate parallel-mode observations. We thank the PACS ICC for their insightful comments on the paper. We acknowledge K. Dassas for making the PSFs available online on the IDOC website. Part of this work has received funding from the European Unions Seventh Framework Programme (FP7/2007-2013) for the DustPedia project (grant agreement No. FP7-SPACE-606847).

References

Bocchio, M., Bianchi, S., Hunt, L. K., & Schneider, R. 2016, A&A, 586, A8
Geis, N., & Lutz, D. 2009, *Herschel*-PACS document PICC-ME-TN-029, v2.2, http://pacs.ster.kuleuven.ac.be/pubtool/PSF/PACSPSF_PICC-ME-TN-029_v1.0.pdf
Lutz, D. 2015, *Herschel*-PACS document PICC-ME-TN-033, v2.2, http://herschel.esac.esa.int/twiki/pub/Public/PacsCalibrationWeb/bolopsf_22.pdf
Okumura, K. 2010, *Herschel*-PACS document SAp-PACS-KO-0716-10 Faint linear artefact in PACS photometer
Ott, S. 2010, in Astronomical Data Analysis Software and Systems XIX, eds. Y. Mizumoto, K.-I. Morita, & M. Ohishi, ASP Conf. Ser., 434, 139
Poglitsch, A., Waelkens, C., Geis, N., et al. 2010, A&A, 518, L2
Roussel, H. 2013, PASP, 125, 1126
Valtchanov, I. 2014, The Spectral and Photometric Imaging Receiver (SPIRE) Handbook, Herschel-Doc-0798, v.2.5, http://herschel.esac.esa.int/Docs/SPIRE/html/spire_om.html